Using Causal Effect Networks to Analyze Different Arctic Drivers of Midlatitude Winter Circulation

MARLENE KRETSCHMER

Potsdam Institute for Climate Impact Research, and Department of Mathematics, University of Potsdam, Potsdam, Germany

DIM COUMOU

Potsdam Institute for Climate Impact Research, Potsdam, Germany

JONATHAN F. DONGES

Potsdam Institute for Climate Impact Research, Potsdam, Germany, and Stockholm Resilience Centre, Stockholm, Sweden

JAKOB RUNGE

Potsdam Institute for Climate Impact Research, Potsdam, and Department of Physics, Humboldt University Berlin, Berlin, Germany

(Manuscript received 11 September 2015, in final form 22 January 2016)

ABSTRACT

In recent years, the Northern Hemisphere midlatitudes have suffered from severe winters like the extreme 2012/13 winter in the eastern United States. These cold spells were linked to a meandering upper-tropospheric jet stream pattern and a negative Arctic Oscillation index (AO). However, the nature of the drivers behind these circulation patterns remains controversial. Various studies have proposed different mechanisms related to changes in the Arctic, most of them related to a reduction in sea ice concentrations or increasing Eurasian snow cover.

Here, a novel type of time series analysis, called causal effect networks (CEN), based on graphical models is introduced to assess causal relationships and their time delays between different processes. The effect of different Arctic actors on winter circulation on weekly to monthly time scales is studied, and robust network patterns are found. Barents and Kara sea ice concentrations are detected to be important external drivers of the midlatitude circulation, influencing winter AO via tropospheric mechanisms and through processes involving the stratosphere. Eurasia snow cover is also detected to have a causal effect on sea level pressure in Asia, but its exact role on AO remains unclear. The CEN approach presented in this study overcomes some difficulties in interpreting correlation analyses, complements model experiments for testing hypotheses involving teleconnections, and can be used to assess their validity. The findings confirm that sea ice concentrations in autumn in the Barents and Kara Seas are an important driver of winter circulation in the midlatitudes.

1. Introduction

The recent cold winters in North America and Eurasia were characterized by a meandering jet stream pattern that allowed cold Arctic air to reach lower latitudes (Cohen et al. 2014b). Moreover, these winters were dominated by a negative phase of the Arctic Oscillation index (AO), which is usually associated with pronounced meridional wind patterns, whereas in a positive AO phase strong zonal flow dominates the wind field. Although a negative AO and meandering flow patterns have been linked to surface extremes (Thompson 2001; Coumou et al. 2014; Screen and Simmonds 2014), it is intensively discussed what the mechanisms behind AO variability are.

Classical atmosphere dynamic theories relate a meandering jet stream structure to above-normal sea

Corresponding author address: M. Kretschmer, Telegrafenberg A62, 14473 Potsdam, Germany.
E-mail: kretschmer@pik-potsdam.de

DOI: 10.1175/JCLI-D-15-0654.1

surface temperatures in the tropical Pacific (Palmer and Mansfeld 1984; Palmer and Owen 1986; Trenberth et al. 1998). Warming of the tropical Pacific intensifies evaporation, increasing thunderstorm activity in that region. The associated latent heat release can then trigger large-amplitude planetary waves, affecting the midlatitude flow.

In contrast, some recently proposed theories focus on the polar region, claiming that anomalous atmospheric circulations can be linked to low Arctic sea ice concentrations as observed during the last two decades (Petoukhov and Semenov 2010; Francis and Vavrus 2012; Jaiser et al. 2012; Handorf et al. 2015). A reduction in sea ice cover in summer leads to the ocean taking up more energy in this season. Since sea ice works as an insulating shield blocking the ocean–atmosphere interaction, less sea ice in autumn and early winter facilitates larger heat fluxes from the relatively warm ocean into the atmosphere. Kim et al. (2014) focus on the Barents and Kara Seas in particular and argue that reduction in sea ice concentration preferentially in this area leads to a weakened AO via the stratospheric polar vortex. They link the additional heat release to the atmosphere caused by sea ice loss in early winter to anomalously high geopotential heights over the Barents and Kara Sea region in addition to lower than normal geopotential heights over northern western Europe and eastern Asia. This observed wavelike structure indicates upward propagation of large-scale planetary waves into the stratosphere, interfering with the predominantly zonal flow in the lower stratosphere. As a result, the stratospheric zonal flow weakens, and the geopotential heights and wind anomalies descend to the troposphere, which is also called a ''breakdown'' of the polar vortex. As a consequence, cold Arctic air reaches lower latitudes, thereby forming large meanders. Those pressure anomalies, respectively meandering of the jet stream, are then most often reflected in a negative phase of AO. Kim et al. (2104) base their analysis on theoretical physical considerations and observational data. They validate their results using climate model simulations, which reproduce similar patterns, supporting their proposed theory.

A similar mechanism was proposed by Cohen et al. (2007, 2013, 2014a), who linked increased fall snow cover in Eurasia to changes in surface pressure anomalies, causing a similar chain of effects. Based on observational data and correlation analysis, they hypothesize that an extended Eurasian snow cover in fall, likely resulting from decreasing Arctic sea ice, leads to increasing sea level pressures over central Asia in early winter. As a result, a disturbed pressure pattern in the polar region is observed, leading to increased vertical wave activity and poleward heat flux. This is followed by anomalously high geopotential heights in the stratosphere, associated with stratospheric warming and weakening of the polar vortex, and, respectively, a negative surface AO, as described by Baldwin and Dunkerton (1999).

To study the atmospheric response to changes in the Arctic, different methods have been used. Cross-correlation analysis is widely applied to detect linear relationships and their time delays between different processes (Polvani and Waugh 2004; Cohen et al. 2014a). However, correlation can be highly biased by autocorrelation effects, by indirect connections via a third process, or by a common driver leading to noncausal, spurious correlations that limits its interpretability (Runge et al. 2014). Also, it does not give any answer on the direction of the relationship so that it is not an adequate tool to study causal effects. Therefore, climate models are used to investigate atmospheric changes due to a controlled perturbation of the system (Deser et al. 2010; Petoukhov and Semenov 2010; Handorf et al. 2015). This approach allows us to interpret results as causal effects forced by the input data. However, conclusions are strictly limited to the extent of the physical realism of the climate model used. It remains questionable whether models capture important processes like ocean–ice feedbacks (Tremblay et al. 2007), land–snow interactions (Furtado et al. 2015), troposphere–stratosphere interactions (Manzini et al. 2014), and Rossby wave propagation (Gray et al. 2014) accurately. Thus, both climate model experiments and correlation analysis of observational data are restricted in their interpretability (Barnes and Screen 2015).

Here, we analyze observational data with a novel method based on graphical models called causal effect networks (CEN). This method overcomes spurious correlations due to autocorrelation, indirect effects, or common drivers (at least among the observed variables included) using a causal discovery algorithm, as proposed by Runge et al. (2012b,a, 2014). This algorithm is a modified version of the Peter Spirtes and Clark Glymour (PC) algorithm (Spirtes et al. 2000), which was first applied to climate research by Ebert-Uphoff and Deng (2012) to study interactions between major climate modes. Causal discovery approaches have since been used to study atmospheric flows (Deng and Ebert-Uphoff 2014), causal relationships in the Walker cell in the tropics (Runge et al. 2014), the monsoonal dynamics in the Pacific–Indian Ocean (Runge et al. 2015), and decadal ocean circulation in the Atlantic (Schleussner et al. 2014).

The aim of this paper is to explain how to apply this method and show how it can be used for hypothesis testing in the context of teleconnections in climate research. We apply CEN to observational and reanalysis data in order to understand how different mechanisms that might

TABLE 1. Table of variables and regions of every considered actor.

Abbreviation	Actor	Variable/unit	Region (level)
BK-SIC	Barents Kara sea ice	Sea ice area fraction	70°–80°N, 30°–105°E
EA-snow	Eurasia snow cover	Snow-covered area fraction	40°–80°N, 30°–180°E
AO	Arctic Oscillation index	Geopotential height (m)	20°–90°N (1000 mb)
v flux	Vertical wave propagation	Poleward eddy heat flux v^*T^* (K m s^{-1})	45°–75°N (100 mb)
PoV	Polar vortex	Geopotential height (m)	65°–90°N (10–100 mb)
Sib-SLP	Siberian High	Sea level pressure (mb)	40°–65°N, 85°–120°E
Ural-SLP	Ural Mountains sea level pressure	Sea level pressure (mb)	45°–70°N, 40°–85°E

cause a negative AO in winter are causally related with each other. In this study, we limit ourselves to testing a set of proposed Arctic mechanisms. In contrast to tropical mechanisms, they operate on similar subseasonal time scales, which facilitates a simultaneous analysis.

The article is structured as follows: In section 2, the data selection is described, and section 3 gives a detailed description of the two different steps of the CEN algorithm on the basis of an example. In section 4, the sensitivity of the parameter settings and temporal resolution is analyzed, and structure and robustness of the graphs are discussed in the framework of the tested hypothesis. Finally, in section 5 we conclude and assess the potentials and limitations of the presented method.

2. Data

Different actors can influence midlatitudinal winter circulation. The first step of our analysis is hence to come up with a reasonable choice of processes that are expected to be relevant for the analysis. This includes the selection of physical variables that should serve as proxies for the considered processes, of suitable data sources, and of a reasonable time resolution of the data.

As stated, we limit the analysis to Arctic processes and follow Kim et al. (2014) and Cohen et al. (2014a) with respect to data selection. We therefore include Barents and Kara sea ice concentrations (BK-SIC) as well as Eurasia snow cover (EA-snow) in our analysis as possible causal drivers of a negative AO. We further include sea level pressure in the Ural Mountains region (Ural-SLP), as defined in (Cohen et al. 2014a) and sea level pressure in the Lake Baikal area as a proxy for Siberian High variability (Sib-SLP). Following Kim et al. (2014) and Cohen et al. (2014a), we include the zonally averaged poleward heat flux v^*T^* at 100 mb (v flux) to capture the troposphere–stratosphere coupling. This is a widely used proxy for vertical wave activity, whereby v denotes the meridional wind velocity, T stands for temperature, and the asterisk denotes deviations from the zonal mean (Polvani and Waugh 2004; Dunn-Sigouin and Shaw 2015). There are many possible ways to describe polar vortex activity (PoV), but for consistency with Kim et al. (2014) and Cohen et al. (2014a) we calculate geopotential height anomalies poleward of 65°N, averaged over pressure levels from 10 to 100 mb to define the strength of the stratospheric polar vortex. Eurasia snow data are described in (Robinson et al. 1993) and are provided by NOAA.[1] Sea ice concentration data were taken from the *Nimbus-7* SMMR and DMSP SSM/I–SSMIS passive microwave dataset provided by the National Snow and Ice Data Center.[2] The AO is provided by NOAA,[3] and for the remaining variables we used ERA-Interim data.[4]

In summary, our analysis contains seven different actors (Table 1): Barents and Kara sea ice concentrations, Eurasia snow cover, the Arctic Oscillation index, vertical wave activity, polar vortex strength, sea level pressure over the Ural Mountains, and Siberian High activity. For each variable, we consider the time period January 1979–December 2014, which is most reliable in the reanalysis because of availability of satellite data.

We calculate monthly means of daily data for each variable, as we are testing mechanisms that are expected to act on monthly time scales. Thereby, we perform linear interpolation of the snow data and for some years of the sea ice concentration dataset, where daily data are not available. To gain additional information on the time scale of the considered processes, we perform additional analysis using half-month means as well as quarter-month means of every variable (Fig. 1). For half-monthly data, we take the mean from the 1st–15th and from the 16th–30th of each month and for February from 1st–14th and 15th–28th, respectively, (thus ignoring the 31st of all applicable months as well

[1] http://gis.ncdc.noaa.gov/all-records/catalog/search/resource/details.page?id=gov.noaa.ncdc:C00756.
[2] http://nsidc.org/data/nsidc-0051.
[3] http://www.cpc.ncep.noaa.gov/products/precip/CWlink/daily_ao_index/ao.shtml.
[4] http://apps.ecmwf.int/datasets/data/interim-full-daily/.

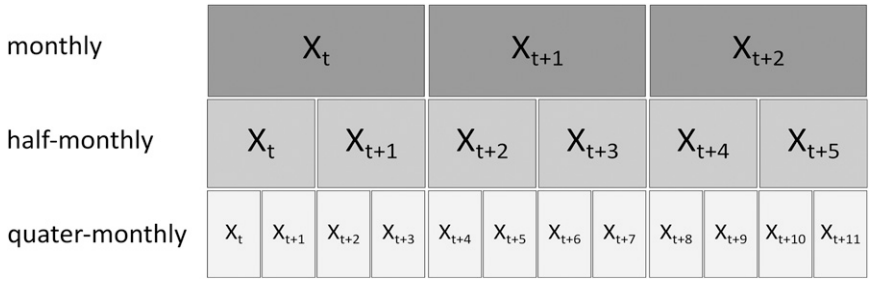

FIG. 1. Schematic picture of different time scales, whereby each box indicates one time step. (bottom) Quarter-monthly time series consists of 4 times and 2 times more data points, respectively, than (top) monthly and (middle) half-monthly time series.

as the 29th of February in leap years). To construct quarter-monthly time series, we calculate the mean from the 1st–7th, 9th–15th, 16th–22nd, and 24th–30th (neglecting hence the 8th, 23rd, and 31st of all applicable months) and for February from the 1st–7th, 8th–14th, 15th–21th, and 22th–28th, respectively. This approach has the advantage that the different time series are still in sync with each other, facilitating the comparison of associated CENs.

For each variable and time resolution, we calculate climatological anomalies (observed value minus the multiyear mean), from which we then compute the area-weighted spatial average over the defined region (see last column in Table 1). This way we create single time series for each time resolution and each actor (see Fig. 2 for monthly data). Since CEN construction requires stationary time series, we remove the linear trend if present. For our analysis this is only the case for BK-SIC. Additionally, we change the sign of PoV such that positive values (negative geopotential height anomalies) indicate a strong polar vortex.

3. Method

The causal effect networks approach is based on two steps: 1) reconstructing the causal parents of each actor using a causal discovery algorithm (Runge et al. 2012a,b, 2014), which is a modification of the PC algorithm (Spirtes et al. 2000) for time series. As explained in the following, this step is based on iterative conditional independence tests using partial correlation. 2) In a second step, the strength of causal links is quantified using a linear version of Pearl's (2013) causal effect measures. Thereby the parents are used in a multiple linear regression analysis to test the significance and strength of causal dependencies between all pairs of actors at a range of time lags.

Here we use a linear approach to estimate and interpret causal links, but the two-step procedure of causal

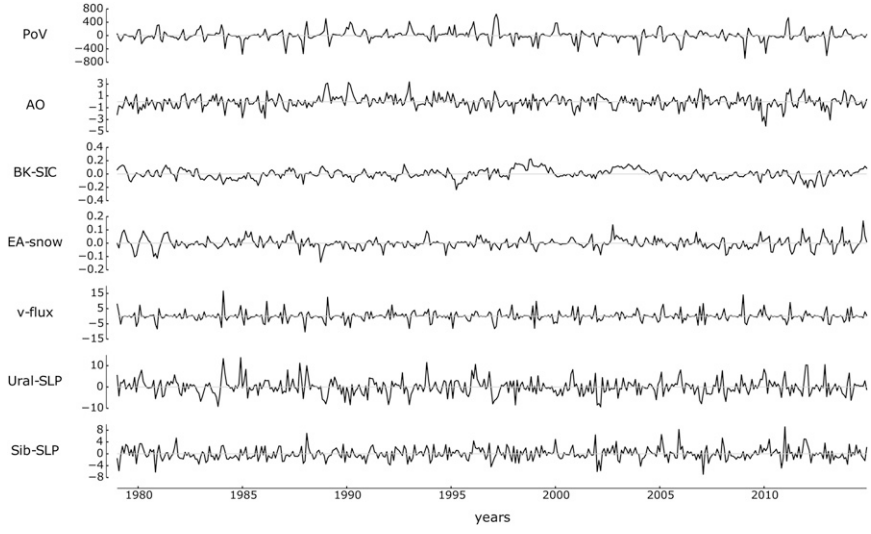

FIG. 2. Monthly time series of all calendar months of climatological anomalies of each actor from January 1979 to December 2014.

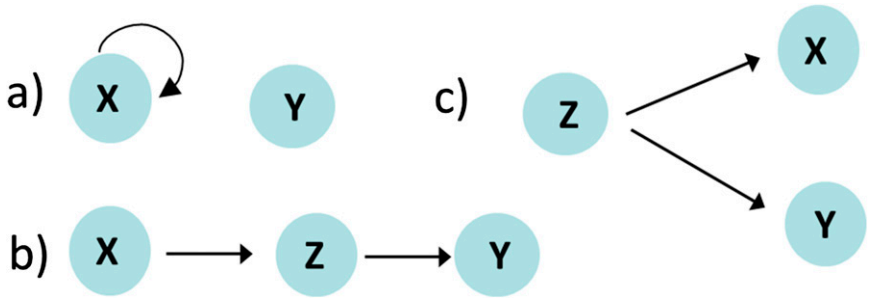

FIG. 3. Possible scenarios leading to a correlation without a direct causation between process X and Y: (a) inflated correlation due to autocorrelation; (b) indirect chain via Z; (c) common driver Z.

reconstruction and quantification can also be embedded in an information–theoretic framework to study causal information transfer accounting for nonlinear relationships between variables. For a detailed explanation of the method, including a mathematical analysis as well as numerical testing, we refer to Runge et al. (2012b,a, 2014). All calculations presented in this study were performed using the Python package Time Series Graph Based Measures of Information Transfer (TiGraMITe), which provides the CEN algorithm and is freely available.[5]

In the following, we explain how to apply CEN to test causality of the hypotheses discussed in the introduction.

a. *Step 1: Detecting causal effects*

The first step of the CEN algorithm aims to find causal relationships between the different actors and their associated time lags. The scope of this step is to identify past processes that directly influence each actor. We call those processes the parents of an actor, and they will be used later to determine the actual strength and the sign of the causal relationships.

Cross correlation can give a first impression of the pairwise linear relationship between two processes X and Y. However, it is not able to identify causal links because the bivariate analysis can be biased by autocorrelation of the two variables, by common drivers, or by indirect links via a third process Z (Figs. 3a,b,c). For example, cross correlation of two independent processes X and Y can be high if one of the processes is strongly autocorrelated (Fig. 3a). Also, imagine that Z causes X and Y (Fig. 3c); then cross-correlation analysis would find a strong correlation between X and Y even though there is no direct link between them. To detect causal links, a multivariate analysis is required, which takes all potential actors into account.

Recall that two processes X and Y are conditionally independent, given a third process Z, if $P(X \cap Y \,|\, Z) = P(X \,|\, Z)P(Y \,|\, Z)$, whereby P denotes the probability function. In the linear case, this can be tested by removing the linear influence of Z from both X and Y and testing for the correlation between their residuals (partial correlation). In the previous case (Fig. 3c), X and Y would then be conditionally independent, given Z. In the example illustrated in Fig. 3b, process X causes Z, which in turn influences Y. Process X and Y are thus conditionally independent, given Z, and a high correlation coefficient between X and Y only occurs because of the indirect link via Z.

This section discusses how the CEN algorithm uses iterative partial correlations to identify noncausal correlations, as depicted in Fig. 3. The extent to which such a databased analysis allows us to conclude on a physical causal mechanism depends on the included variables, time resolution of the data, and assumptions, such as stationarity. Two free parameters are involved: the significance level α for the partial correlation tests and the maximum time delay $\tau_{\max}$.

CALCULATING THE PARENT PROCESSES

As an illustrative example, we start with finding those processes on a monthly time scale among our actors that have a direct causal effect on the winter [December–February (DJF)] PoV. We look at the monthly time series for every actor (Fig. 2), having thus a sample length of 108 time steps. We define a two-sided significance level $\alpha = 0.01$ and a maximum time lag of $\tau_{\max} = 3$ months, implying that parent processes more than three months ago or those with a significance below 99% will be neglected.

First, for every actor X, the cross-correlation function $\rho(X_{t-\tau}, \mathrm{PoV}_t)$ is calculated for time shifts of $\tau = 1$ up to the maximum time shift $\tau_{\max} = 3$ months. Note that, if we study causal effects on winter PoV, this implies that the monthly time series PoV_t only consists of winter data, but the lagged or driving variable contains data from other seasons (in particular, autumn, but also summer when $\tau > 3$). Here, the expression "driver" is

[5] https://www.pik-potsdam.de/members/jakrunge.

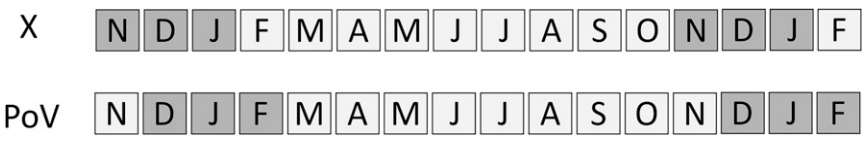

FIG. 4. Schematic picture of time series considered to measure influence of actor X on winter PoV with a time lag $\tau = 1$, whereby the time series only consist of the dark gray boxes.

used in its statistical meaning of being conditional dependent and shifted in time. For $\tau = 1$, the expression $\rho(X_{t-1}, \mathrm{PoV}_t)$ denotes the Pearson correlation coefficient of November–January data of process X and December–February data of PoV (see Fig. 4), whereas for $\tau = 3$ the linear influence of the three months shifted September–November data of actor X on PoV in winter (DJF) is measured. For example, for the influence of Eurasia snow cover (X = EA-snow) on the polar vortex with a time delay of $\tau = 1$, we obtain:

$$\rho(\text{EA-snow}_{t-1}, \text{PoV}_t) = -0.262,$$

which is significant at the $\alpha = 0.01$ level. This indicates that there is a negative linear relationship between early winter [November–January (NDJ)] snow and the winter polar vortex. This seems reasonable since a large snow cover in Eurasia is indicated to induce a weakened polar vortex (Cohen et al. 2014a). The cross-correlation function is now calculated and evaluated for every actor $X \in \{\text{BK-SIC}_{t-\tau}, \text{EA-snow}_{t-\tau}, \text{AO}_{t-\tau}, \upsilon\,\text{flux}_{t-\tau}, \text{PoV}_{t-\tau}, \text{Sib-SLP}_{t-\tau}, \text{Ural-SLP}_{t-\tau}\}$ and every time lag $\tau \in \{1, 2, 3\}$. We find that, besides EA-snow (with $\tau = 1$), also Ural-SLP (with $\tau = 1$ and $\tau = 2$), AO (with $\tau = 1$), PoV (with $\tau = 1$), and υ flux (with $\tau = 1$) are significantly correlated with winter PoV. Sorted by the strength of correlation starting with the strongest in absolute value, the set of potential parent processes of PoV in this zeroth iteration step without any conditioning is:

$$\mathbf{P}^0 = \{\upsilon\ \text{flux}_{t-1}, \text{PoV}_{t-1}, \text{Ural-SLP}_{t-1}, \text{Ural-SLP}_{t-2}, \text{AO}_{t-1}, \text{EA-snow}_{t-1}\}.$$

To test these potential drivers for conditional independence, we next calculate partial correlations:

$$\rho(X_{t-\tau}, Y_t \,|\, \mathbf{Z}),$$

which measure the linear influence from process X on Y, excluding the influence of some set of variables $\mathbf{Z}$. This thus checks if X and Y are conditionally independent given $\mathbf{Z}$. We choose $\mathbf{Z}$ as a subset of $\mathbf{P}^0$ such that $\mathbf{Z}$ denotes a set of other processes that potentially influences the bivariate correlation coefficient $\rho(X_{t-\tau}, Y_t)$. In each iteration step $\mathbf{P}^1, \mathbf{P}^2, \ldots$, we condition on a new $\mathbf{Z}$, whereby the algorithm first takes only one condition and starts with the process that is strongest correlated (in absolute value) with process Y. Then the dimension of the subset selected from the remaining parents is increased, and different two-dimensional conditions are tested, and so on for higher dimensions. If the partial correlation significance test of a pair $X_{t-\tau}$ and Y_t is nonsignificant given $\mathbf{Z}$, the process $X_{t-\tau}$ is removed from the set of potential parents. If, however, the partial correlation $\rho(X_{t-\tau}, Y_t \,|\, \mathbf{Z})$ remains significant for all tested $\mathbf{Z}$, then actor X is considered to directly influence Y with a time lag of τ.

Returning to our example, we first test condition $\mathbf{Z} = \{\upsilon\ \text{flux}_{t-1}\}$ and find

$$\rho(\text{EA-snow}_{t-1}, \text{PoV}_t \,|\, \upsilon\ \text{flux}_{t-1}) = -0.147,$$

which is not significantly different from zero at our chosen level, and hence we find that EA-snow and PoV are conditionally independent (at a time delay of one month) if the influence of υ flux from the same time shift is excluded. We thus conclude that there is no direct influence from EA-snow on PoV with a delay of one month and that the significant correlation between them $\rho(\text{EA-snow}_{t-1}, \text{PoV}_t) = -0.261$ is due to the influence of υ flux. For example, EA-snow could be linked to PoV indirectly via υ flux (as in Fig. 3b). On the other hand, if we take $X = \text{Ural-SLP}_{t-1} \in \mathbf{P}^0$ and condition on the same $\mathbf{Z} = \{\upsilon\ \text{flux}_{t-1}\}$, we find

$$\rho(\text{Ural-SLP}_{t-1}, \text{PoV}_t \,|\, \upsilon\ \text{flux}_{t-1}) = -0.281$$

which is still significantly different from zero. In other words, the linear influence of Ural-SLP$_{t-1}$ on PoV$_t$ cannot exclusively be explained by the linear influence of υ flux.

We calculate partial correlations for all the elements from $\mathbf{P}^0$ conditioning on $\mathbf{Z} = \{\upsilon\ \text{flux}_{t-1}\}$ and find that some of them are conditionally independent from PoV given υ flux$_{t-1}$, which can thus be neglected as potential

drivers of winter PoV. This way we obtain a much smaller set of potential parent processes of PoV:

$$\mathbf{P}^1 = \{\upsilon\ \text{flux}_{t-1}, \text{PoV}_{t-1}, \text{Ural-SLP}_{t-1}\} \subset \mathbf{P}^0.$$

Now the algorithm proceeds by conditioning on the process that was second strongest correlated with PoV: that is, $\mathbf{Z} = \{\text{PoV}_{t-1}\}$. We thus check if some of the potential drivers of PoV only occur because of the autocorrelation of PoV. Calculating partial correlations of the elements of $\mathbf{P}^1$ conditioning on $\mathbf{Z} = \{\text{PoV}_{t-1}\}$ gives only values significantly different from zero such that $\mathbf{P}^2 = \mathbf{P}^1$. The last possibility of picking only one condition is $\mathbf{Z} = \{\text{Ural-SLP}_{t-1}\}$, where we find again that all the partial correlations remain significantly different from zero such that $\mathbf{P}^3 = \mathbf{P}^2 = \mathbf{P}^1$. Sorting the elements by the strength of their partial correlation value in the last iteration step, we have

$$\mathbf{P}^3 = \{\upsilon\ \text{flux}_{t-1}, \text{Ural-SLP}_{t-1}, \text{PoV}_{t-1}\}.$$

Now we increase the dimension of $\mathbf{Z}$ and condition on two possible drivers from $\mathbf{P}^3$. Thus, we start with $\mathbf{Z} = \{\upsilon\ \text{flux}_{t-1}, \text{Ural-SLP}_{t-1}\} \subset \mathbf{P}^3$ and calculate

$$\rho(\text{PoV}_{t-1}, \text{PoV}_t \,|\, \upsilon\ \text{flux}_{t-1}, \text{Ural-SLP}_{t-1}) = 0.268,$$

which is still significantly different from zero. When testing for the other possibilities ($\mathbf{Z} = \{\upsilon\ \text{flux}_{t-1}, \text{PoV}_{t-1}\}$ and $\mathbf{Z} = \{\text{Ural-SLP}_{t-1}, \text{PoV}_{t-1}\}$), the partial correlations remain significant. Since there are no more combinations for choosing $\mathbf{Z}$, the algorithm converges and stops.

We have now found the set of direct drivers of winter PoV (relative to the variables taken into account), which we call its parents, denoted by

$$\mathbf{P}_{\text{PoV}} = \{\upsilon\ \text{flux}_{t-1}, \text{Ural-SLP}_{t-1}, \text{PoV}_{t-1}\}.$$

In other words, we found that (given the settings of $\tau_{\max} = 3$ and $\alpha = 0.01$) winter PoV is directly driven by itself with a delay of one month and by υ flux and Ural-SLP with a delay of one month but is (linearly) conditionally independent of all other processes.

The procedure described for PoV is performed for all actors, yielding a set of parents for every actor (see Table 2):

$$\mathbf{P} = \{\mathbf{P}_{\text{AO}}, \mathbf{P}_{\text{BK-SIC}}, \mathbf{P}_{\text{EA-snow}}, \mathbf{P}_{\upsilon\ \text{flux}}, \mathbf{P}_{\text{PoV}}, \mathbf{P}_{\text{Sib-SLP}}, \mathbf{P}_{\text{Ural-SLP}}\}.$$

Note that the interpretation of the significance level α as the probability of false rejections of the hypothesis of a noncausal link is not strictly valid here since we tested every possible link multiple times by conditioning on different processes (see discussion section).

TABLE 2. Table of parent processes of each actor for winter (DJF) data and with the settings $\alpha = 0.01$ and $\tau_{\max} = 3$. The subscript denotes the time lag in months. The parent processes are then used in the second step of the CEN algorithm in order to quantify the link strength in terms of linear regression coefficients.

Actor	Parents $\mathcal{P}$
AO	AO_{t-1}, BK-SIC_{t-2}
BK-SIC	BK-SIC_{t-1}, PoV_{t-2}
EA-snow	EA-snow_{t-1}
υ flux	PoV_{t-1}
PoV	$\upsilon\ \text{flux}_{t-1}$, Ural-SLP_{t-1}, PoV_{t-1}
Sib-SLP	None
Ural-SLP	BK-SIC_{t-3}

b. Step 2: Quantifying causal effects

In the second step, we use the sets of parents to determine the strength of causal relationships. The case of $\tau = 0$ (i.e., when there is no time shift between the actors) was omitted when calculating the parents. In this step, we will nevertheless quantify the significant instantaneous relationships conditional on the parents. As stated above, such contemporaneous links can, in general, not be interpreted in a causal way. Some might turn out to be causal parents at a higher time resolution, but some might be just due to excluded common drivers. We address this issue later by studying different time lags.

As mentioned, the set of derived parents depends on the significance level α, which here, however, cannot be well interpreted because of the multiple testing problem. To better assess significance, we therefore test every possible combination of actors and time lags again (including links from parents) using the causal parents as a conditioning set.

In general, multiple linear regression can be used to measure the influence a system of variables (the independent variables) has on a different (dependent) variable. However, it can often be challenging to define a set of independent variables that can explain the dependent variable. The list of causal parents provides a reasonable choice for those variables with their associated time lags. We calculated the link strength using standardized multiple linear regression coefficients based on our list of parents for the case of $\alpha = 0.01$ and up to a maximum lag of $\tau_{\max} = 3$. We found that PoV is influenced from the past by $\mathcal{P}_{\text{PoV}} = \{\upsilon\ \text{flux}_{t-1}, \text{Ural-SLP}_{t-1}, \text{PoV}_{t-1}\}$. To calculate if process X significantly influences PoV with a time lag of $\tau \geq 0$, we formulate the standardized linear regression model

$$\text{PoV}_t^* = \beta_0 + \beta_1(\upsilon\ \text{flux}_{t-1}^*) + \beta_2 \text{Ural-SLP}_{t-1}^* + \beta_3 \text{PoV}_{t-1}^* + \beta_4 X_{t-\tau}^* + \varepsilon.$$

Here the beta coefficients β_i with $i \in \{0, 1, 2, 3, 4\}$ denote the standardized regression coefficients, ε stands for the error term, and the asterisk indicates that the time series have been normalized and standardized. The regression coefficients express how much the different independent variables contribute to variability in PoV in terms of standard deviations. Interpreted causally (Pearl 2013), this means that if X is increased by one standard deviation, keeping the other variables fixed, then PoV increases by β_4 standard deviations. The β coefficient of X is tested for significance at $\alpha = 0.01$ with the null hypothesis $\beta = 0$, which would mean that variable X does not contribute significantly to the dependent variable PoV.

To test if, for example, X = EA-snow significantly influences winter PoV with a delay of one month $\tau = 1$, we calculate the standardized linear regression model and choose EA-snow$_{t-1}$ as well as the parents of PoV as independent variables to explain PoV:

$$\text{PoV}^*_t = \beta_0 + \beta_1 \upsilon\,\text{flux}^*_{t-1} + \beta_2 \text{Ural-SLP}^*_{t-1} + \beta_3 \text{PoV}^*_{t-1} + \beta_4 \text{EA-snow}^*_{t-\tau} + \varepsilon.$$

We get $\beta_4 = -0.076$, which is not significant at the $\alpha = 0.01$ level such that the influence from EA-snow on PoV with a delay of one month is considered to be absent. If we, however, calculate the influence of υ flux with $\tau = 1$ (which is also in $\mathcal{P}_{\text{PoV}}$) on winter PoV, we obtain a significant beta coefficient $\beta_1 = -0.514$. Thus, υ flux is concluded to be causally influencing the winter polar vortex with a delay of one month and with a strength of $\beta_1 = -0.514$; that is, a one-standard deviation increase in υ flux leads to a negative change of about half a standard deviation in PoV.

We test the influence of every actor $X \in \{\text{BK-SIC}_{t-\tau}, \text{EA-snow}_{t-\tau}, \text{AO}_{t-\tau}, \upsilon\,\text{flux}_{t-\tau}, \text{PoV}_{t-\tau}, \text{Sib-SLP}_{t-\tau}, \text{Ural-SLP}_{t-\tau}\}$ and every time lag $\tau \in \{0, 1, 2, 3\}$ on PoV as well as on every other actor in the form of standardized linear regression. The remaining significant links form our causal effect network.

Note, it is possible that, in this step, significant direct links are identified that had been rejected in the first step. Nevertheless, by testing every potential link again, we can better interpret the statistical meaning of α as the probability of falsely rejecting the null hypothesis that a lagged variable $X_{t-\tau}$ is independent of Y_t given the parents of Y_t selected with the causal algorithm. However, we will see that our list of parents strongly coincides with the significant strong links identified in the second step.

4. Results and discussion

We construct CEN for winter circulation and with different α and $\tau_{\max}$ settings. Visualization of CEN as a process graph gives an easy to interpret picture of the underlying complex teleconnection pattern. Only the significant links are presented in the graph, and the numbers next to the links stand for the associated time lag τ. Instantaneous links are represented by dashed links and have no direction or time shift. The node color (in case the variable influences itself) and the link color represent the standardized regression coefficient (beta values) and hence capture the strength of the causal relationship. If two processes are linked for more than one time lag, then all lags are given (sorted by strength), with the link color based on the strongest connection. The time lag for autodriven data is not shown in the graph, but predominantly actors are lag-1 autocorrelated.

For the settings $\alpha = 0.01$ and $\tau_{\max} = 3$ and using monthly data, we obtain the CEN as in Fig. 5a. We find evidence that BK-SIC have a negative effect on Ural-SLP with a time delay of three months. Thus, low sea ice in autumn can lead to increased surface pressure in winter. We also find a positive link between Ural-SLP and υ flux with a delay of one month, which means that higher surface pressure can increase the poleward heat flux and, respectively, the vertical wave activity. This is consistent with the mechanisms proposed by Cohen et al. (2014a) and Kim et al. (2014). Moreover, we can see in Fig. 5a, that increasing vertical wave activity induces a weakening of the stratospheric polar vortex with a delay of one month. Hence, the CEN depicts the troposphere–stratosphere coupling described by Kim et al. (2014) and Cohen et al. (2014a). We also see a reverse relation from the stratosphere into the troposphere, whereby a weak PoV leads to increasing sea ice in the Barents and Kara Seas and to less vertical wave activity. We find no causal link connecting a weak polar vortex to a negative AO. However, we have a positive instantaneous link between them, which might indicate that this connection is happening on a submonthly time scale. In addition to the mechanisms involving the stratosphere, we also detect a direct positive link from BK-SIC to AO. Thus, we find that Barents and Kara sea ice in fall induces a weakening of AO in winter without any stratospheric connection. However, AO is also instantaneously related to Ural-SLP with a negative sign, which is in turn strongly positively related with Sib-SLP. Even though the instantaneous links provide no direction, they are in accordance with the expectation that AO is negative when sea level pressure in the Arctic is high. The same is true for the instantaneous links connecting Sib-SLP and Ural-SLP to each other with respect to BK-SIC. In addition to the influence of Ural-SLP on PoV via υ flux, we also find a weaker direct causal link between them with a delay of one month,

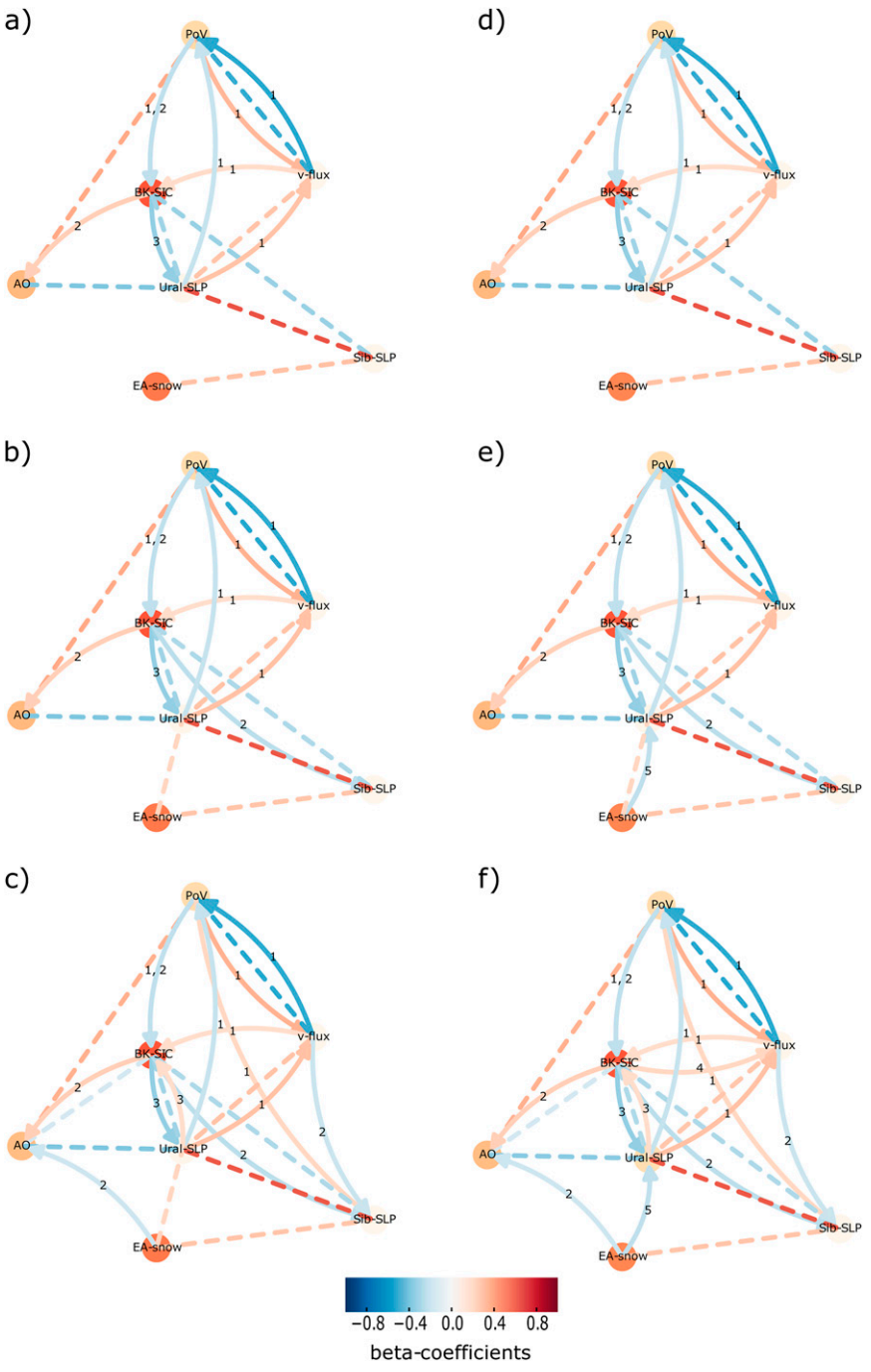

FIG. 5. CENs of actors of winter (DJF) circulation based upon monthly mean data. With a maximum time lag of (a)–(c) $\tau_{max} = 3$ and (d)–(f) $\tau_{max} = 5$ and with significance levels (a),(d) $\alpha = 0.01$, (b),(e) $\alpha = 0.025$, and (c),(f) $\alpha = 0$.

suggesting that high sea level pressure in central Asia can induce a weakening of the polar vortex directly, or via processes which are not part of the tested hypothesis. The positive instantaneous link between EA-snow and Sib-SLP is indicating that increasing snow cover in Eurasia is associated with a strengthened Siberian High, which is consistent with the hypothesis of Cohen et al. (2014a). The autoregressive influence (with a time lag of one month) is, as expected, especially high for BK-SIC and EA-snow and weaker for PoV and AO. Ural-SLP, Sib-SLP, and v flux are not significantly causally influenced by their values in the months before.

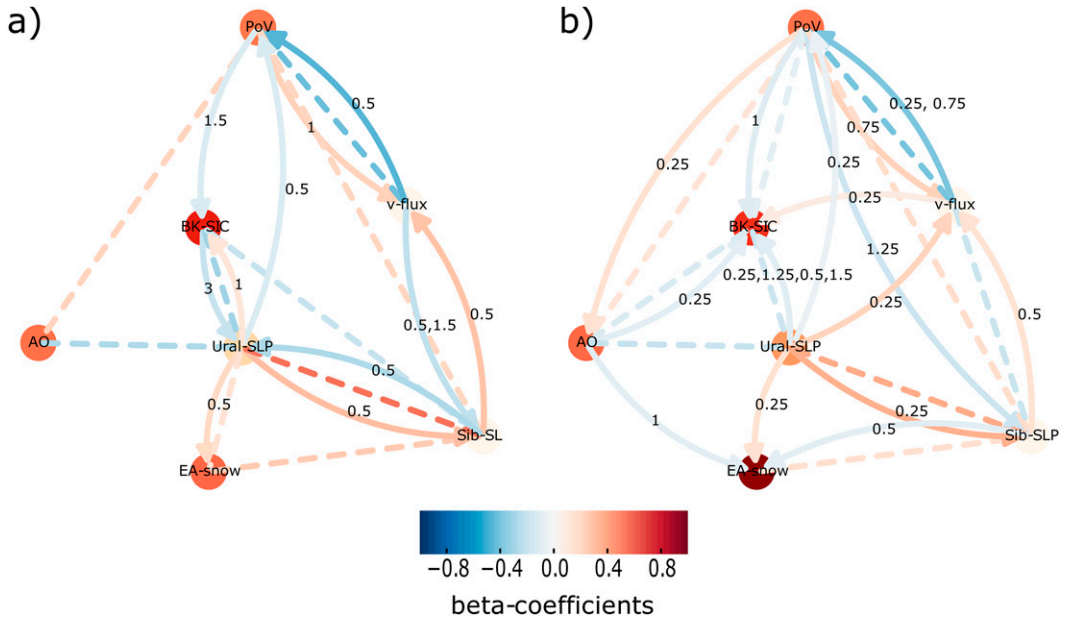

FIG. 6. CEN of actors of winter (DJF) circulation for (a) half-monthly data with $\tau_{max} = 6$ and $\alpha = 0.005\,625$ and (b) quarter-monthly data with $\tau_{max} = 12$ and $\alpha = 0.003$.

We performed sensitivity analyses of the CEN to the parameter settings used and found the detected links to be robust. We limit ourselves to analyzing only links that go back to late summer. Figure 5 shows the winter months CENs associated with different significance levels ($\alpha = 0.01$, 0.025, and 0.05 in the rows) and for maximum time lags of three and five months (columns). Not surprisingly, the number of significant links increases when we increase α, most of them involving the two actors based on sea level pressure (Figs. 5b,e,c,f). Also, links associated with time lags of more than three months (Figs. 5d–f) appear when increasing the maximum time lag τ_{max}, however only for larger α values. We see that all links in Fig. 5a appear in all other graphs as well. For a significance level $\alpha > 0.01$ (Figs. 5b,e,c,f), we see that decreasing BK-SIC induces stronger Sib-SLP with a lag of two months. This is in accordance with the mechanism described by Kim et al. (2014). We also see for $\alpha > 0.01$ that increasing EA-snow is also instantaneously positively linked to Ural-SLP. For a longer time lag, we find that EA-snow is negatively influencing sea level pressure in the Ural-SLP with a delay of five months (Figs. 5e,f). For $\alpha = 0.05$, we even find some evidence that EA-snow can influence AO directly, and thus it seems again that processes not involving the stratosphere are present. Overall, the CEN structure as in Fig. 5a appears for all tested parameters.

As explained in the method section, instantaneous links provide no information on the direction. To gain further information on the direction of those links and to further test the robustness of our findings, we construct CENs also for half-monthly and quarter-monthly time series (see Figs. 6a,b). Since the datasets are then 2 times and 4 times longer, respectively, and consist of shorter time steps, we adjust our settings for the CEN algorithm. To make the results comparable with Fig. 5a, we therefore double and quadruple τ_{max}, respectively, to refer to the same time shift. Since for higher time resolutions more potential links are tested for significance, we adjust the α value accordingly.[6] Comparing Fig. 5a with CENs based on half-monthly (Fig. 6a) and quarter-monthly (Fig. 6b) time series with the same maximum time shift of three months and an adjusted significance level $\alpha = 0.005\,625$ for half-monthly and $\alpha = 0.003$ for quarter-monthly data, we find a robust pattern of the involved causal processes. Especially the troposphere–stratosphere connection is clearly visible in all CENs. For the CEN based on half-monthly data (Fig. 6a) the connection to vertical wave propagation (v flux) is via the Siberian region (Sib-SLP), whereby this region is directly influenced by the Ural Mountains (Ural-SLP) area. On a quarter-monthly time scale, both regions directly influence v flux, which in turn influences PoV (Fig. 6b). On the

[6] If n denotes the number of actors, then $N = n^2(\tau_{max} + 1) - n$ potential links are tested. Thus, $N = 189$ (monthly), $N = 336$ (half monthly) and $N = 630$ (quarter monthly). To calculate the adapted α, we use a simple Bonferroni correction and divide $\alpha = 0.01$ by the multiplicity of the performed tests.

other hand, we have a direct link from PoV to AO (Fig. 6b) in the quarter-monthly based CEN, which indicates that a weakening of the polar vortex causes a negative AO on a weekly time scale. Also, there are direct links connecting Ural-SLP to EA-snow, BK-SIC, and Sib-SLP, which shows that the Ural Mountains region has a strong influence on the surrounding regions on submonthly time scales, which is in accordance with the tested hypothesis. However, the strong instantaneous links between tropospheric-based actors (AO, Ural-SLP, Sib-SLP, and EA-snow) remain for all time scales, indicating that those causal processes are occurring on subweekly time scales or are due to common drivers. The darker node colors show that, at submonthly time scales, autoregressive processes become larger.

In summary, the CEN algorithm provides robust results, whereby additional links can predominantly be explained by changing parameter settings and by the temporal resolution of the underlying time series. Barents and Kara sea ice is detected to play an important role on winter circulation, especially on the monthly time scale (Fig. 5), both by being responsible for changes in the pressure profile over the Ural Mountains region and by influencing AO directly. Thus, mechanisms effecting AO not involving the stratosphere seem to be important too. We assume that other processes, for example, as described by Petoukhov and Semenov (2010), not represented by our choice of actors play a role, connecting Arctic sea ice and AO. As stated by Cohen and Kim, we find a connection of surface pressure (Ural-SLP) and upward wave activity (υ flux) into the stratosphere for all parameter settings and time scales (Figs. 5, 6). On lower time scales, we also have a direct link from Sib-SLP to υ flux (Fig. 6). These findings confirm the hypothesis that higher pressure over central Asia leads to increasing vertical wave activity into the stratosphere (Cohen et al. 2014a). The Ural Mountains region as a preferred location for atmospheric blocking (Wang et al. 2009) seems to play a central role for winter circulation, being linked to the tropospheric actors AO, BK-SIC, Sib-SLP, and EA-snow on all time scales. Further, the region is responsible for coupling with the stratosphere (Figs. 5, 6). In this context, we expect that the link connecting Ural-SLP to PoV directly, and not via υ flux, can at least partly be explained by hemispheric-wide averaging of the actors υ flux and PoV (in contrast to the regional actor Ural-SLP). Additionally, it is possible that a common driver not included in this analysis is responsible for this direct link. For example, tropical teleconnections like ENSO could influence both the Arctic stratosphere and sea level pressure in central Asia (Butler et al. 2014). Additionally, we find that the increased vertical wave activity can induce a weakening of the PoV, whereas PoV is positively connected to surface AO (Figs. 5, 6). Thus, our findings are consistent with the troposphere–stratosphere–troposphere mechanisms described by Cohen et al. (2014a) and Kim et al. (2014). We also find a reverse connection, linking a weak PoV to increasing Barents and Kara sea ice and decreasing υ flux. This provides a negative feedback on a time scale of approximately one to two months. The role of EA-snow seems to be more complex. We find no evidence that late autumn snowfall in Eurasia influences the sea level pressure in central Asia, as proposed by Cohen et al. (2014a). However, we find that EA-snow is instantaneously linked to Sib-SLP with positive sign and for $\alpha > 0.01$ also to Ural-SLP (Figs. 5, 6). On a monthly time scale, we also have a direct negative link to Ural-SLP (with a lag of five months) and for $\alpha = 0.05$ also to AO (with a lag of two months). Overall, our findings are less robust for EA-snow.

5. Conclusions

In the context of hypothesis testing, we constructed causal effect networks (CEN) in order to unravel causal relationships and their time delays between different actors of midlatitude winter circulation. We restricted ourselves to studying Arctic mechanisms, based on those proposed by Kim et al. (2014) and Cohen et al. (2014a). For each of the seven actors, we constructed one index at different temporal resolutions. CEN construction was performed by first deriving a set of parents for each actor, consisting of the conditional dependent processes (step 1). Then those parents were used to estimate the strength and statistical significance of links employing linear regression models (step 2). We only considered effects on winter circulation and applied the method to monthly, half-monthly, and quarter-monthly time series. We found that the method provides robust results for different values of the significance level α and maximum time delay $\tau_{\max}$ as well as for the considered range of temporal resolutions.

Figure 7 (respectively, Fig. 5a) contains the most robust links on a monthly scale, whereby results are presented according to the approximate geographical location of the actors. Overall, our findings are largely consistent with previously proposed hypotheses under consideration, whereby especially Barents and Kara sea ice is detected to be an important external driver for winter circulation. Our CENs confirm the proposed troposphere–stratosphere coupling, which is evident for all tested parameter settings. However, we also find a robust pattern indicating a direct tropospheric connection of Barents and Kara sea ice and AO, as, for example, proposed by Petoukhov and Semenov (2010). The direct link connecting Ural-SLP to PoV might be due to unconsidered tropical mechanisms influencing

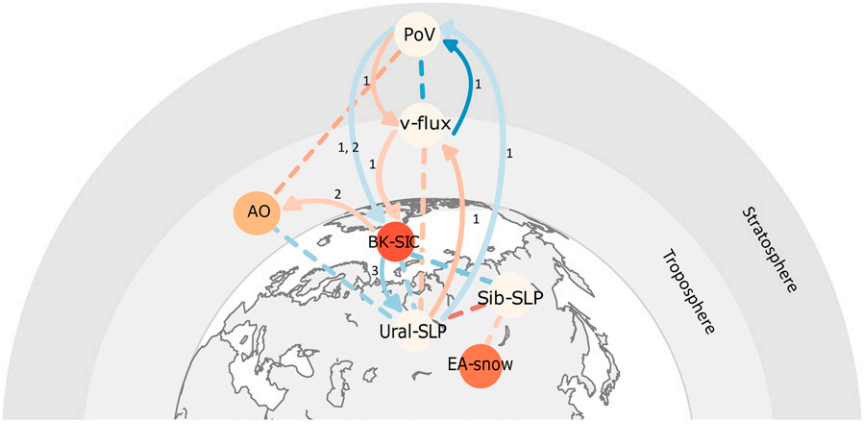

FIG. 7. As in Fig. 5a, but the network is embedded in a schematic projection of the earth and the atmosphere. The regional actors BK-SIC, Ural-SLP, Sib-SLP, and EA-snow are presented according to their approximate geographical location, and the hemispheric actors AO, v flux, and PoV are presented according to their approximate latitude and pressure levels. See Table 1 for the exact coordinates of all actors.

both the stratosphere and sea level pressure in Eurasia, as documented by Butler et al. (2014). The role of Eurasia snow cover is less robust but seems to influence sea level pressure in Asia significantly.

Since the CEN algorithm requires the choice of the free parameters $\tau_{\max}$ and α and depends on the temporal resolution of the underlying data, changing settings can produce different graphs. However, by including sensitivity tests for different parameter settings and time scales, we report robust results. Also, it should be noted that the CEN approach assumes stationary time series. Long-term trends or changing trends within the studied time period might affect the results (Overland and Wang 2005) and require a careful treatment of the data. However, here we only found a clear negative linear trend in the sea ice data. The causal interpretation of the resulting CENs also depends on the choice of actors such that the inferred parents can still be due to not-yet-included other variables. The challenge of how to choose adequate actors can also be assessed by different methods, such as dimension reduction via principal component analysis (Runge et al. 2015). Nonetheless, the CEN algorithm is especially useful for testing hypotheses if consistency of the data choice is assured.

The scope of this paper was to introduce and explain the CEN algorithm and how it can be applied to address questions associated with teleconnections in the global climate system. In this context, CENs can overcome ambiguities of correlation analyses and provide a practical supplemental method to model experiments in order to test hypotheses. Moreover, CENs could be used also on model data to assess their validity. Here we limited ourselves to linear measurements, but CENs can also be constructed using nonparametric approaches (e.g., from information theory) (Runge et al. 2012b,a). Further research should address the question of how tropical mechanisms contribute to midlatitude winter circulation (Palmer 2014; Trenberth et al. 2014) and also the different hypotheses related to summer circulation (Overland et al. 2012; Coumou et al. 2015).

Acknowledgments. The authors thank the editor and three anonymous reviewers for constructive and insightful comments that helped to significantly improve the manuscript. The work was supported by the German Federal Ministry of Education and Research (Grant 01LN1304A). J. R. received support by the German Federal Ministry of Science and Education (Young Investigators Group CoSy-CC^2, Grant 01LN1306A). J. F. D. thanks the Stordalen Foundation (via the Planetary Boundary Research Network PB.net) and the Earth League's EarthDoc program for financial support.

REFERENCES

Baldwin, M. P., and T. J. Dunkerton, 1999: Propagation of the Arctic Oscillation from the stratosphere to the troposphere. *J. Geophys. Res.*, **104**, 30 937–30 946, doi:10.1029/1999JD900445.

Barnes, E. A., and J. A. Screen, 2015: The impact of Arctic warming on the midlatitude jet-stream: Can it? Has it? Will it? *Wiley Interdiscip. Rev.: Climate Change*, **6**, 277–286, doi:10.1002/wcc.337.

Butler, A. H., L. M. Polvani, and C. Deser, 2014: Separating the stratospheric and tropospheric pathways of El Niño–Southern Oscillation teleconnections. *Environ. Res. Lett.*, **9**, 024014, doi:10.1088/1748-9326/9/2/024014.

Cohen, J., M. Barlow, P. J. Kushner, and K. Saito, 2007: Stratosphere–troposphere coupling and links with Eurasian land surface variability. *J. Climate*, **20**, 5335–5343, doi:10.1175/2007JCLI1725.1.

——, J. Jones, J. C. Furtado, and E. Tziperman, 2013: Warm Arctic, cold continents. *Oceanography*, **26** (4), 1–12, doi:10.5670/oceanog.2013.70.

——, J. C. Furtado, J. Jones, M. Barlow, D. Whittleston, and D. Entekhabi, 2014a: Linking Siberian snow cover to precursors of stratospheric variability. *J. Climate*, **27**, 5422–5432, doi:10.1175/JCLI-D-13-00779.1.

——, and Coauthors, 2014b: Recent Arctic amplification and extreme mid-latitude weather. *Nat. Geosci.*, **7**, 627–637, doi:10.1038/ngeo2234.

Coumou, D., V. Petoukhov, S. Rahmstorf, S. Petri, and H. J. Schellnhuber, 2014: Quasi-resonant circulation regimes and hemispheric synchronization of extreme weather in boreal summer. *Proc. Natl. Acad. Sci. USA*, **111**, 12 331–12 336, doi:10.1073/pnas.1412797111.

——, J. Lehmann, and J. Beckmann, 2015: The weakening summer circulation in the Northern Hemisphere mid-latitudes. *Science*, **348**, 324–327, doi:10.1126/science.1261768.

Deng, Y., and I. Ebert-Uphoff, 2014: Weakening of atmospheric information flow in a warming climate in the Community Climate System Model. *Geophys. Res. Lett.*, **41**, 193–200, doi:10.1002/2013GL058646.

Deser, C., R. Tomas, M. Alexander, and D. Lawrence, 2010: The seasonal atmospheric response to projected Arctic sea ice loss in the late twenty-first century. *J. Climate*, **23**, 333–351, doi:10.1175/2009JCLI3053.1.

Dunn-Sigouin, E., and T. A. Shaw, 2015: Comparing and contrasting extreme stratospheric events, including their coupling to the tropospheric circulation. *J. Geophys. Res. Atmos.*, **120**, 1374–1390, doi:10.1002/2014JD022116.

Ebert-Uphoff, I., and Y. Deng, 2012: Causal discovery for climate research using graphical models. *J. Climate*, **25**, 5648–5665, doi:10.1175/JCLI-D-11-00387.1.

Francis, J. A., and S. J. Vavrus, 2012: Evidence linking Arctic amplification to extreme weather in mid-latitudes. *Geophys. Res. Lett.*, **39**, L06801, doi:10.1029/2012GL051000.

Furtado, J. C., J. L. Cohen, A. H. Butler, E. E. Riddle, and A. Kumar, 2015: Eurasian snow cover variability and links to winter climate in the CMIP5 models. *Climate Dyn.*, **45**, 2591–2605, doi:10.1007/s00382-015-2494-4.

Gray, S. L., C. M. Dunning, J. Methven, G. Masato, and J. M. Chagnon, 2014: Systematic model forecast error in Rossby wave structure. *Geophys. Res. Lett.*, **41**, 2979–2987, doi:10.1002/2014GL059282.

Handorf, D., R. Jaiser, K. Dethloff, A. Rinke, and J. Cohen, 2015: Impacts of Arctic sea ice and continental snow cover changes on atmospheric winter teleconnections. *Geophys. Res. Lett.*, **42**, 2367–2377, doi:10.1002/2015GL063203.

Jaiser, R., K. Dethloff, D. Handorf, A. Rinke, and J. Cohen, 2012: Impact of sea ice cover changes on the Northern Hemisphere atmospheric winter circulation. *Tellus*, **64A**, 11595, doi:10.3402/tellusa.v64i0.11595.

Kim, B.-M., S.-W. Son, S.-K. Min, J.-H. Jeong, S.-J. Kim, X. Zhang, T. Shim, and J.-H. Yoon, 2014: Weakening of the stratospheric polar vortex by Arctic sea-ice loss. *Nat. Commun.*, **5**, 4646, doi:10.1038/ncomms5646.

Manzini, E., and Coauthors, 2014: Northern winter climate change: Assessment of uncertainty in CMIP5 projections related to stratosphere-troposphere coupling. *J. Geophys. Res.*, **119**, 7979–7998, doi:10.1002/2013JD021403.

Overland, J. E., and M. Wang, 2005: The Arctic climate paradox: The recent decrease of the Arctic Oscillation. *Geophys. Res. Lett.*, **32**, L06701, doi:10.1029/2004GL021752.

——, J. A. Francis, E. Hanna, and M. Wang, 2012: The recent shift in early summer Arctic atmospheric circulation. *Geophys. Res. Lett.*, **39**, L19804, doi:10.1029/2012GL053268.

Palmer, T. N., 2014: Record-breaking winters and global climate change. *Science*, **344**, 803–804, doi:10.1126/science.1255147.

——, and D. A. Mansfeld, 1984: Response of two atmospheric general circulation models to sea-surface temperature anomalies in the tropical East and West Pacific. *Nature*, **310**, 483–485, doi:10.1038/310483a0.

——, and J. A. Owen, 1986: A possible relationship between some "severe" winters in North America and enhanced convective activity over the tropical west Pacific. *Mon. Wea. Rev.*, **114**, 648–651, doi:10.1175/1520-0493(1986)114<0648:APRBSW>2.0.CO;2.

Pearl, J., 2013: Linear models: A useful "microscope" for causal analysis. *J. Causal Inference*, **1**, 155–170, doi:10.1515/jci-2013-0003.

Petoukhov, V., and V. A. Semenov, 2010: A link between reduced Barents-Kara sea ice and cold winter extremes over northern continents. *J. Geophys. Res.*, **115**, D21111, doi:10.1029/2009JD013568.

Polvani, L. M., and D. W. Waugh, 2004: Upward wave activity flux as a precursor to extreme stratospheric events and subsequent anomalous surface weather regimes. *J. Climate*, **17**, 3548–3554, doi:10.1175/1520-0442(2004)017<3548:UWAFAA>2.0.CO;2.

Robinson, D. A., K. F. Dewey, and R. R. Heim, 1993: Global snow cover monitoring: An update. *Bull. Amer. Meteor. Soc.*, **74**, 1689–1696, doi:10.1175/1520-0477(1993)074<1689:GSCMAU>2.0.CO;2.

Runge, J., J. Heitzig, N. Marwan, and J. Kurths, 2012a: Quantifying causal coupling strength: A lag-specific measure for multivariate time series related to transfer entropy. *Phys. Rev.*, **86**, 061121, doi:10.1103/PhysRevE.86.061121.

——, ——, V. Petoukhov, and J. Kurths, 2012b: Escaping the curse of dimensionality in estimating multivariate transfer entropy. *Phys. Rev. Lett.*, **108**, 258701, doi:10.1103/PhysRevLett.108.258701.

——, V. Petoukhov, and J. Kurths, 2014: Quantifying the strength and delay of climatic interactions: The ambiguities of cross correlation and a novel measure based on graphical models. *J. Climate*, **27**, 720–739, doi:10.1175/JCLI-D-13-00159.1.

——, and Coauthors, 2015: Identifying causal gateways and mediators in complex spatio-temporal systems. *Nat. Commun.*, **6**, 8502, doi:10.1038/ncomms9502.

Schleussner, C. F., J. Runge, J. Lehmann, and A. Levermann, 2014: The role of the North Atlantic overturning and deep ocean for multi-decadal global-mean-temperature variability. *Earth Syst. Dyn.*, **5**, 103–115, doi:10.5194/esd-5-103-2014.

Screen, J. A., and I. Simmonds, 2014: Amplified mid-latitude planetary waves favour particular regional weather extremes. *Nat. Climate Change*, **4**, 704–709, doi:10.1038/nclimate2271.

Spirtes, P., C. Glymour, and R. Scheines, 2000: *Causation, Prediction, and Search*. Bradford, 568 pp.

Thompson, D. W. J., 2001: Regional climate impacts of the Northern Hemisphere annular mode. *Science*, **293**, 85–89, doi:10.1126/science.1058958.

Tremblay, L. B., M. M. Holland, I. V. Gorodetskaya, and G. A. Schmidt, 2007: An ice-free Arctic? Opportunities for computational science. *Comput. Sci. Eng.*, **9**, 65–74, doi:10.1109/MCSE.2007.45.

Trenberth, K. E., G. W. Branstator, D. Karoly, A. Kumar, N.-C. Lau, and C. Ropelewski, 1998: Progress during TOGA in understanding and modeling global teleconnections associated with tropical sea surface temperatures. *J. Geophys. Res.*, **103**, 14 291–14 291, doi:10.1029/97JC01444.

——, J. T. Fasullo, G. Branstator, and A. S. Phillips, 2014: Seasonal aspects of the recent pause in surface warming. *Nat. Climate Change*, **4**, 911–916, doi:10.1038/nclimate2341.

Wang, L., W. Chen, W. Zhou, J. C. L. Chan, D. Barriopedro, and R. Huang, 2009: Effect of the climate shift around mid 1970s on the relationship between wintertime Ural blocking circulation and East Asian climate. *Int. J. Climatol.*, **30**, 153–158, doi:10.1002/joc.1876.